UNIVERSITÀ
DEGLI STUDI
DI PADOVA

Università degli Studi di Padova

Padua Research Archive - Institutional Repository

Magnetic properties of epsilon iron(III) oxide nanorod arrays functionalized with gold and copper(II) oxide

(Article begins on next page)

Magnetic properties of ε iron(III) oxide nanorod arrays functionalized with gold and copper(II) oxide

Chiara Maccato,[1] Giorgio Carraro,[1,*] Davide Peddis,[2] Gaspare Varvaro,[2,*] Davide Barreca[3]

[1] *Department of Chemistry, Padova University and INSTM, 35131 Padova, Italy*

[2] *CNR-ISM, Monterotondo Scalo (Roma), 00015, Italy*

[3] *CNR-ICMATE and INSTM, Department of Chemistry, Padova University, 35131 Padova, Italy.*

* Corresponding authors; e-mail: giorgio.carraro@unipd.it, gaspare.varvaro@ism.cnr.it

Abstract

A sequential chemical vapor deposition (CVD) - radio frequency (RF)-sputtering approach was adopted to fabricate supported nanocomposites based on the scarcely investigated ε-iron(III) oxide polymorph. In particular, ε-Fe_2O_3 nanorod arrays were obtained by CVD, and their subsequent functionalization with Au and CuO nanoparticles (NPs) was carried out by RF-sputtering under mild operational conditions. Apart from a multi-technique characterization of material structure, morphology and chemical composition, particular efforts were dedicated to the investigation of their magnetic properties. The pertaining experimental data, discussed in relation to the system chemico-physical characteristics, are directly dependent on the actual chemical composition, as well as on the spatial distribution of Au and CuO nanoparticles. The approach adopted herein can be further implemented to control and tailor different morphologies and phase compositions of iron oxide-based nanomaterials, meeting thus the open requests of a variety of technological utilizations.

Keywords: epsilon iron oxide; gold; copper; magnetic properties.

1. Introduction

Nanomaterials based on iron(III) oxides, eventually functionalized with metal or metal-oxide nanoparticles (NPs), are attractive platforms for various technological applications, encompassing biomedicine, (photo)catalysis, solar assisted H_2 generation, gas sensing/batteries, and magnetic devices [1-7]. To this regard, due to the search for iron oxide-based nanomaterials endowed with specific features, the scarcely investigated ferrimagnetic ε-Fe_2O_3 polymorph has emerged for its peculiar properties with respect to the most stable and widely studied γ-Fe_2O_3 and α-Fe_2O_3 [8-12]. Indeed, ε-Fe_2O_3 nanomaterials diplay a superior activity in solar-assisted photocatalytic process [2-3,13-14] and intriguing magnetic properties, such as giant room-temperature coercive field, that can be exploited for the fabrication of electric/magnetic field or multiple-state memory devices [1,15-18]. In this context, a considerable attention has been devoted to the possibility of boosting material performances by suitable surface functionalization, that represents a strategic option for the development of multi-functional systems to be exploited in various tecnological applications [4]. In particular, various routes have been developed, such as grafting or coating with organic molecules, polymers, and biomolecules, or functionalization with inorganic species [1,3-4,9,16-17]. Indeed, a precise engineering of the resulting interfaces can not only exert a protective action over the underlying Fe_2O_3, but also result in the birth of improved and/or unprecedented chemical, physical and functional characteristics [3,13-14,16,19].

In this framework, the functionalization of magnetic iron oxide systems with Au NPs yields various advantages, including the stabilization of magnetic Fe_2O_3 under corrosive biological conditions. In addition, the controlled introduction of well dispersed Au nanoparticles affords magnetic systems endowed with plasmonic properties, rendering Fe_2O_3-Au composite systems important candidates for various end uses, such as magnetic, photocatalytic, optical and biomedical applications [14,20-24]. Equally and otherwise interesting is the functionalization of

magnetic iron oxide nanosystems with CuO NPs. CuO, an antiferromagnetic p-type semiconductor ($E_G \approx 1.2$ eV) with a Néel temperature of 230 K [25-26], has a broad perspective of applications as active component in superconductors and electrode materials, as well as in field emitters, solar cells, and photocatalysts [27-30]. As a matter of fact, ε-Fe$_2$O$_3$-CuO composites represent attractive multifunctional materials with tuneable magnetic properties [25,31-32].

In order to meet the open scientific and technological demands, the availability of versatile fabrication and processing techniques, enabling material fabrication under controlled conditions onto suitable substrates, is highly demanded [1,8,10,16,23,33-35], especially for ε-Fe$_2$O$_3$-Au and ε-Fe$_2$O$_3$-CuO materials. In fact, the systhesis of supported single phase ε-Fe$_2$O$_3$ nanosystems with tailored nano-organization is still a challenging issue. Recently, our group has developed a CVD process for the selective preparation of ε-Fe$_2$O$_3$ nanosystems with tailored nano-organization [15,36]. In the present study, we report on the preparation of ε-Fe$_2$O$_3$-Au and ε-Fe$_2$O$_3$-CuO nanocomposites through a two-step preparative approach. The proposed route consists in the initial CVD of supported ε-Fe$_2$O$_3$ nanorods arrays, followed by the subsequent deposition of Au or CuO NPs by radio frequency (RF)-sputtering at low temperatures and applied powers, to avoid detrimental alterations of the pristine iron oxide matrix [14,32,37]. After a multi-technique characterization aimed at assessing structural, morphological, and compositional properties, the magnetic behaviour of the obtained composites was investigated and discussed, with particular focus on the role of Au and CuO nanoparticles. To the best of our knowledge, no previous reports on the magnetic properties of the target materials are available in the literature up to date.

2. Experimental

2.1 Synthesis

A cold-wall CVD horizontal equipment was adopted for the preparation of iron(III) oxide nanorod arrays, using Fe(hfa)$_2$TMEDA (hfa = 1,1,1,5,5,5-hexafluoro-2,4-pentanedionate; TMEDA = N,N,N',N'–tetramethylethylenediamine) as a molecular source (vaporization temperature = 60 °C) [38]. Precursor vapors were delivered by an O$_2$ flow (purity = 6.0; rate = 100 sccm) into the reaction chamber through connection gas lines maintained at 120°C in order to prevent detrimental condensation processes. An additional oxygen flow (100 sccm), passing through a water reservoir heated at 50°C, was independently introduced into the CVD reactor. Depositions were performed on pre-cleaned 1×1 cm^2 Si(100) substrates (MEMC®, Merano, Italy), using the following experimental settings: substrate temperature = 400 °C; total pressure = 10.0 mbar; deposition time = 60 min. The CVD conditions have been selected starting from our previous studies [36], in order to obtain single phase ε-Fe$_2$O$_3$ nanosystems.

Subsequently, as-prepared iron oxide samples were mounted into a two-electrode reaction system [39] for RF-sputtering (ν = 13.56 MHz), that was conducted using pure Ar as plasma source. In particular, RF-sputter deposition of gold was performed using an Au metal target (BAL-TEC AG, 99.99%) under the following conditions: substrate temperature = 60°C; RF-power = 5 W; total operating pressure = 0.3 mbar; Ar flow rate = 10 sccm; duration = 40 min. RF-sputter deposition of copper(II) oxide was carried out using a copper target (Alfa Aesar®; purity = 99.95 %) under the same conditions adopted for gold, apart from the process duration (90 min). The adopted conditions were optimized in a series of preliminary experiments in order to control the overall Au (CuO) content and prevent a complete coverage of the underlying iron oxide matrices, as well as the occurrence of their undesired alterations.

2.2 Characterization

X-ray Diffraction (XRD) measurements were carried out on a Dymax-RAPID X-ray microdiffractometer using Cu Kα radiation.

Field Emission-Scanning Electron Microscopy (FE-SEM) mesurements were carried out at primary beam acceleration voltages comprised between 10 and 20 kV by means of a Zeiss SUPRA 40VP instrument.

X-ray Photoelectron Spectroscopy (XPS) analyses were performed by a Perkin Elmer Φ 5600ci spectrometer with a standard Al Kα source (1486.6 eV), at a working pressure lower than 10^{-8} mbar. The reported binding energy (BE) values were corrected for charging effects by assigning a BE of 284.8 eV to the adventitious C1s peak, as reported in previous publications [40-41]. After a Shirley-type background subtraction [42], atomic percentages (at.%) were evaluated using sensitivity factor values provided by Φ V5.4 A software. The Cu Auger (α) parameter was calculated by using the following equation:

$$\alpha_{Cu} = BE(Cu2p_{3/2}) + KE(CuLMM) \tag{1}$$

with KE = kinetic energy [40-41]. The Auger parameter was used as a finger-print to unambiguously identify copper oxidation state, since it is indipendent on any static charging and can be measured with a greater accuracy than the core level BE or Auger peaks. In fact, since the chemical shifts of photoelectrons and Auger electrons are different, the difference between their kinetic energies constitutes a special spectral property, and its numerical value is unique for each chemical state [43-44]. The comparison of Auger parameter values with the reference ones tabulated in specialized handbook or databases enables thus to identify the element oxidation state with high accuracy [40-41,45].

Au/Cu molar fractions were defined as [32]:

$$X_M = (M\ at.\%)/[(M\ at.\%) + (Fe\ at.\%)] \tag{2}$$

5

Room temperature magnetic properties were carefully investigated by combining quasi-static field- and angle-dependent magnetization and remanent measurements performed using a vibrating sample magnetometer (model 10-MicroSense, $H_{max} = 20\,\text{kOe}$). In particular, besides field-dependent magnetization loops measured along the direction parallel and perpendicular to the rod axis, advanced measurement protocols were used to investigate the magnetic interaction and the reversal mechanism.

3. Results and Discussion

In the present work, the main attention was initially devoted to investigate the structure, mophology and composition of $\varepsilon\text{-Fe}_2\text{O}_3$-Au and $\varepsilon\text{-Fe}_2\text{O}_3$-CuO nanosystems, with particular regard to the composition and distribution of Cu- and Au-containing NPs.

Fig. 1 shows the XRD patterns of the target systems, revealing the formation of $\varepsilon\text{-Fe}_2\text{O}_3$ as the only iron(III) oxide polymorph. In particular, the peaks located at $2\vartheta = 18.7°, 30.1°, 33.1,°$ $34.8°$, and $37.8°$ could be assigned respectively to the (002), (013), (122), (113) and (211) reflections of orthorhombic $\varepsilon\text{-Fe}_2\text{O}_3$ [46] as the sole iron(III) oxide polymorph. As already discussed in our previous works [2,36], a key role for the selective obtainment of $\varepsilon\text{-Fe}_2\text{O}_3$ nanomaterials is the introduction of water into the reaction atmosphere, significantly affecting the overall process. In fact, water introduction results in a diffusion-controlled process, promoting the formation of $\varepsilon\text{-Fe}_2\text{O}_3$ deposits [36], and induces the formation of oxygen defects, that play a key role in the growth and stabilization of the metastable $\varepsilon\text{-Fe}_2\text{O}_3$ phase [2]. In a different way, in the presence of dry O_2, a surface-reaction-limited regime CVD process occurs, leading to the formation of $\beta\text{-Fe}_2\text{O}_3$ systems.

A comparison of the relative peak intensities with the reference powder spectrum suggested the occurrence of a preferential [013] orientation (see also below and Fig. 5) [36]. No significant microstructural variations occurred upon functionalization with Au or CuO NPs, due to the high

dispersion and low amount of the latter species. This observation, in line with previous reports [14,32], was also confirmed by the data obtained through other characterization techniques (see below).

The morphological organization was investigated by FE-SEM analyses, highlighting the presence of porous nanorod arrays, aligned perpendicularly with respect to the Si(100) substrate surface, with mean lateral size and length of (60 ± 10) nm and (520 ± 20) nm, respectively (Fig. 2). Both the the pseudo-conic tips and the spiral-like rod shape suggested the occurrence of a spiral dislocation growth mechanism, promoted by the system tendency to decrease the total free energy [32,36,47]. The anisotropic growth responsible for the formation of these pillar-like structures was in agreement with the preferential [013] orientation evidenced by XRD analyses.

Upon functionalization with Au (or CuO) NPs, the iron oxide morphology was almost preserved thanks to the use of mild sputter deposition conditions. In Fe_2O_3-Au composites, Au nanoparticles with an average size of (15 ± 3) nm could be clearly detected on the iron oxide tips, suggesting a three dimensional (*Volmer−Weber*) growth mode, as already reported for Au deposition on oxide supports [37,48]. Upon CuO sputter deposition, a careful inspection of higher magnification images in Fig. 2 showed that nanometer-sized CuO NPs were deposited both on the tips of ε-Fe_2O_3 nanorods and along the entire wire walls, thanks to the porosity of the obtained nanorod arrays. This different distribution could be traced back to a higher chemical affinity of CuO NPs with ε-Fe_2O_3 with respect to the case of metallic gold NPs. Indeed, this difference was considered as the main responsible for the higher in-depth penetration of CuO nanoparticles [14,32].

The system chemical composition was investigated by XPS analyses. Fig. 3 compares XPS wide-scan spectra for ε-Fe_2O_3-CuO and ε-Fe_2O_3-Au nanosystems, that were dominated by iron and **oxygen peaks**, along with a minor carbon signal (< 10 at.%) due to adventitious contamination [41]. The presence of iron(III) oxide free from other Fe oxidation states was

confirmed by the Fe2p signal [BE(Fe2p$_{3/2}$) = 711.1 eV; spin–orbit splitting = 13.7 eV, Fig. 3a. The O1s signal (not shown) resulted from the contribution of lattice oxygen in Fe_2O_3 (and also in CuO for the Fe_2O_3-CuO sample; BE = 530.0 eV) and surface –OH species (BE = 531.8 eV) [15,36,41,45]. Accordingly, the O/Fe atomic ratio was slightly higher than the expected stoichiometric value. For the ε-Fe_2O_3-Au sample, Au photoelectron peaks were well evident, and the Au4f$_{7/2}$ BE (84.5 eV) confirmed the presence of metallic gold NPs (Fig. 3b) [28,41,45]. As a matter of fact, this BE value resulted to be ≈0.4 eV higher than the typical ones reported for metallic gold, a phenomenon related to both charge exchange and relaxation/screening phenomena [14,48]. Regarding the ε-Fe_2O_3-CuO specimens (Fig. 3c), the formation of Cu(II) oxide was evidenced by: i) the Cu2p peak position [BE(Cu2p$_{3/2}$) = 934.1 eV]; ii) the presence of *shake-up* satellites at BE ≈9.0 eV higher than the principal spin orbit components; iii) the value of the Auger parameter (α_{Cu} = 1851.5 eV) [30,32,41,45]. Calculations of molar fractions yielded similar values for Au and Cu (X_{Au} = 0.5; X_{Cu} = 0.6).

A preliminary invesigation of NP effects on the magnetic behavior of ε-Fe_2O_3 rods was performed by recording at 300 K the field-dependent magnetization loops along the directions parallel and perpendicular to the rod axis (Fig. 4). The larger hysteresis observed along the perpendicular direction indicated that the magnetization preferentially alingns along the normal to the rod axis, which represents the direction of minimum energy, *i.e.* the magnetic easy-axis. To explain the observed magnetic anisotropy symmetry, the two main contributions to the effective anisotropy were taken into account: the magneto-crystalline anisotropy ($\boldsymbol{K_{mc}}$), closely related to the material structure and symmetry, and the shape anisotropy ($\boldsymbol{K_{sh}}$), that would favour the magnetization alignment along the rod axis. The large magneto-crystalline anisotropy of ε-Fe_2O_3 phase ($\boldsymbol{K_{mc}}$≈0.2–0.5 MJ×m^{-3}) [18] significantly overcomes the shape anisotropy arising from the elongated rod shape, being the upper limit for an uniformly magnetized and infinite wire equal to $\boldsymbol{K_{sh} = 1/2\,\mu_0 M_s^2}$ ≈ 3.5–10 kJ×m^{-3} (where M_s≈75–125 kA×m is the saturation

magnetization [18]). On this basis, it can be suggested that the magneto-crystalline anisotropy represents the main contribution for the presently investigated systems. The preferential [013] rod orientation, as detected by XRD analysis, indicates that the a-axis of the ε-Fe_2O_3 orthorhombic cell corresponding to the magnetic easy-axis associated to the magnetocrystalline anisotropy [16,49], is mainly directed along the normal to the rod axis (Fig. 5), explaining thus the observed anisotropy simmetry. In addition, also the dipolar interaction among the rods could contribute to the development of a magnetic easy-axis perpendicular to the rod axis itself [50]. It is worthwhile noticing that, along the easy-axis direction, both the samples did not reach a saturation state even under an external applied field of ≈ 2 T. This phenomenon was related to the lack of ferrimagnetic and/or to the relative low value of the maximum available field, insufficient to reach saturation due to the high ε-Fe_2O_3 magneto-crystalline anisotropy [15]. Although the magnetic phase is the same in both the samples, ε-Fe_2O_3-Au exhibited a nearly single-phase behavior, whereas ε-Fe_2O_3-CuO showed a constricted hysteresis loop along the normal to the rod axis, which indicated the co-existence of two magnetic phases with different anisotropy. Since bare ε-Fe_2O_3 rods showed a single-phase behavior [15], such a result suggested that the nanoparticle decoration played a key role in determining the final system properties. The addition of NPs could degrade the magnetic propeties of the rod surface, which became magnetically softer, the strenght of this effect depending on the coverage degree. In the case of ε-Fe_2O_3-Au, metal particles were mostly confined on the top of the rods, thus leading to a small effect, whereas lower sized CuO particles were distributed along the whole rod axes, increasing the amount of the softer phase and explaining thus the constricted hysteresis loop observed in this case.

To further disclose the effects of nanoparticle introduction, in-plane remanence magnetization studies were performed to investigate the magnetic interactions between the rods. Both Isothermal Remanent Magnetization (IRM) and Direct Current Demagnetization (DCD) remanent magnetization curves were measured (Fig. 6a). The initial state for an IRM

measurement is a totally demagnetized sample cooled in zero magnetic field. In the present case, an external field was applied for 10 s; subsequently, it was switched off and the remanence was measured (M_{IRM}). The process was repeated, increasing the field up 2 T. In a DCD measurement, the initial state is the magnetically saturated one. An external field of -2 T was applied for 10 s; then, a small external field in the direction opposite to magnetization was applied and, after 10 s, it was switched off and the remanent magnetization (M_{DCD}) was measured. By differentiating the two remanence curves with respect to the field, it is possible to obtain the irreversible susceptibility χ_{irr}. The latter represents a map of the switching field distribution in both IRM and DCD modes where the switching field is the magnetic field needed to irreversibly revert the magnetization. For an ideal, non-interacting system with unixial anisotropy the two differentiated curves should overlap, with a factor of 2 in the height of the $dM_{r,IRM}/dH$ relative to the $dM_{r,DCD}/dH$ curve derived from the Wohlfarth relation [51]:

$$M_{r,DCD} = 1 - 2M_{r,IRM} \tag{3}$$

In a real system, any deviation from this relationship can be attributed to the effect of magnetic interactions as proposed by Kelly [52], who expressed the parameter δM as:

$$\delta M = M_{r,DCD} - (1 - 2M_{r,IRM}) \tag{4}$$

Positive δM values can be attributed to interactions promoting the magnetized state (exchange interactions), whereas negative δM values are due to demagnetizing interactions (*e.g.*, dipole-dipole interactions) [53]. It is worth recalling that exchange interactions imply a direct contact between magnetic elements, whereas the dipolar interactions are long-range ones and are directly (inversely) proportional to the moment (distance). The remanence measurements (Fig. 6b) indicated that dipolar interactions were predominant in all the samples (negative δM), the absolute value of δM (*i.e.*, the interaction strength) being larger for ε-Fe$_2$O$_3$-Au ($\delta M \approx 0.31$) and lower for ε-Fe$_2$O$_3$-CuO ($\delta M \approx 0.24$). The lower dipolar interaction strength in the Fe$_2$O$_3$-CuO

sample could be a consequence of a magnetization reduction due to a variation of magnetic properties at the rod surface. In order to attain a deeper insight into the sample magnetic behavior, the magnetization reversal (or switching) mechanism of sample Fe_2O_3-Au, which presents a nearly single-phase behavior, was investigated by measuring a set of DCD curves at different ϕ angles (ranging between 0° and 90°, Fig. 7a), ϕ being the angle between H and the magnetic easy-axis, *i.e.* the normal to the rod axis in the target case. The remanent curves allow purely irreversible magnetization changes to be investigated and are more appropriate to describe the switching process with respect to the hysteresis loops, that encompass both reversible and irreversible processes [54]. From each DCD curve, the remanent coercivity H_{cr}, defined as the field at which the remanence is zero, was determined and its dependence as a function of the angle ϕ (*i.e.*, H_{cr} *vs.* ϕ) is reported in Fig. 7b. The observed trend suggested a highly incoherent magnetization reversal process, which can explain the lower values of coercivity (≈0.35 T) and remanence coercivity (≈0.75 T) with respect to typical ones reported for randomly oriented single-domain ε-Fe_2O_3 nanoparticles reversing coherently [55].

4. Conclusions

The present contribution reported on the vapor phase preparation of ε-Fe_2O_3 nanorod arrays functionalized with Au (or CuO) nanoparticles. In particular, Si(100)-supported ε-Fe_2O_3 deposits were obtained by a CVD route, and functionalization with gold [or copper(II) oxide] nanoparticles was subsequently performed by RF-sputtering under mild conditions. The obtained materials were characterized by the formation of oriented ε-Fe_2O_3 nanorod arrays, with Au NPs mainly concentrated in the outermost system region, whereas CuO nanoaggregates were distributed even in the inner regions. For the first time, the magnetic properties of supported ε-Fe_2O_3-Au and ε-Fe_2O_3-CuO composites were investigated, revealing the occurrence of various effects that could be attributed to the performed NPs functionalization. In particular, when the rods were decorated

with Au nanoparticles, their magnetic properties remained almost unchanged, being the particles mainly confined on the top of the rods. In a different way, CuO nanoparticle decorated the whole rod walls, leading to an appreciable variation of magnetic properties. The obtained results open attractive perspectives for further advancements of the present research activities, concerning a deeper insight into the relations between the NP nature/nano-organization and the resulting magnetic properties. Such studies can promote both fundamental and applied developments towards the exploitation of ε-Fe$_2$O$_3$, eventually functionalized by metallic of metal oxide NPs, in various tecnological applications, such as information storage devices, energy, telecommunications, and biomedicine.

References

[1] M. Yoshikiyo, A. Namai, K. Nakagawa, S.-i. Ohkoshi, Magnetic glass-film based on single-nanosize AIP Adv. 7 (2017) 056218.

[2] G. Carraro, C. Maccato, A. Gasparotto, T. Montini, S. Turner, O.I. Lebedev, V. Gombac, G. Adami, G. Van Tendeloo, D. Barreca, P. Fornasiero, Enhanced hydrogen production by photoreforming of renewable oxygenates through nanostructured Fe_2O_3 polymorphs, Adv. Funct. Mater. 24 (2014) 372.

[3] L.T. Quynh, C.N. Van, Y. Bitla, J.W. Chen, T.H. Do, W.Y. Tzeng, S.C. Liao, K.A. Tsai, Y.C. Chen, C.L. Wu, C.H. Lai, C.W. Luo, Y.J. Hsu, Y.H. Chu, Self-Assembled $BiFeO_3$-ε-Fe_2O_3 Vertical Heteroepitaxy for Visible Light Photoelectrochemistry, Adv. Energy Mater. 6 (2016) 10.1002/aenm.201600686.

[4] W. Wu, Q. He, C. Jiang, Magnetic iron oxide nanoparticles: synthesis and surface functionalization strategies, Nanoscale Res. Lett. 3 (2008) 397-415.

[5] R. Cornell, U. Schwertmann, The Iron Oxides, 2nd Edition ed., Wiley-VCH GmbH & Co., Weinheim, 2003.

[6] G. Muscas, G. Singh, W.R. Glomm, R. Mathieu, P.A. Kumar, G. Concas, E. Agostinelli, D. Peddis, Tuning the size and shape of oxide nanoparticles by controlling oxygen content in the reaction environment: morphological analysis by aspect maps, Chem. Mater. 27 (2015) 1982-1990.

[7] L. Suber, D. Peddis, Approaches to synthesis and characterization of spherical and anisometric metal oxide magnetic nanomaterials. In Nanomaterials for life science, Kumar, C. S. S. R., Ed. Wiley: 2010; Vol. 4, p 431475.

[8] V.N. Nikolić, M. Tadić, M. Panjan, L. Kopanja, N. Cvjetićanin, V. Spasojević, Influence of annealing treatment on magnetic properties of Fe_2O_3/SiO_2 and formation of ε-Fe_2O_3 phase, Ceram. Int. 43 (2017) 3147-3155.

[9] D.A. Balaev, S.S. Yakushkin, A.A. Dubrovskii, G.A. Bukhtiyarova, K.A. Shaikhutdinov, O.N. Martyanov, Study of the high-coercivity material based on ε-Fe_2O_3 nanoparticles in the silica gel matrix, Techn. Phys. Lett. 42 (2016) 347-350.

[10] A. Sivkov, E. Naiden, A. Ivashutenko, I. Shanenkov, Plasma dynamic synthesis and obtaining ultrafine powders of iron oxides with high content of ε-Fe_2O_3, J. Magn. Magn. Mater 405 (2016) 158-168.

[11]   D. Korte, G. Carraro, F. Fresno, M. Franko, Thermal properties of surface-modified α- and ε-Fe_2O_3 photocatalysts determined by beam deflection spectroscopy, Int. J. Thermophys. 35 (2014) 2107-2114.

[12]   C. Cannas, A. Ardu, D. Niznansky, D. Peddis, G. Piccaluga, A. Musinu, Simple and fast preparation of pure maghemite nanopowders through sol–gel self-combustion, J. Sol-Gel Sci. Technol. 60 (2011) 266-274.

[13]   D. Barreca, G. Carraro, A. Gasparotto, C. Maccato, F. Rossi, G. Salviati, M. Tallarida, C. Das, F. Fresno, D. Korte, U. Lavrenčič Štangar, M. Franko, D. Schmeisser, Surface functionalization of nanostructured Fe_2O_3 polymorphs: from design to light-activated applications, ACS Appl. Mater. Interfaces 5 (2013) 7130-7138.

[14]   G. Carraro, A. Gasparotto, C. Maccato, V. Gombac, F. Rossi, T. Montini, D. Peeters, E. Bontempi, C. Sada, D. Barreca, P. Fornasiero, Solar H_2 generation via ethanol photoreforming on epsilon-Fe_2O_3 nanorod arrays activated by Ag and Au nanoparticles, RSC Adv. 4 (2014) 32174-32179.

[15]   G. Carraro, D. Barreca, C. Maccato, E. Bontempi, L.E. Depero, C. de Julian Fernandez, A. Caneschi, Supported and β iron oxide nanomaterials by chemical vapor deposition: structure, morphology and magnetic properties, CrystEngComm 15 (2013) 1039-1042.

[16]   S.-i. Ohkoshi, A. Namai, T. Yamaoka, M. Yoshikiyo, K. Imoto, T. Nasu, S. Anan, Y. Umeta, K. Nakagawa, H. Tokoro, Mesoscopic bar magnet based on ε-Fe_2O_3 hard ferrite, Sci. Rep. 6 (2016) 27212.

[17]   O.S. Ivanova, R.D. Ivantsov, I.S. Edelman, E.A. Petrakovskaja, D.A. Velikanov, Y.V. Zubavichus, V.I. Zaikovskii, S.A. Stepanov, Identification of ε-Fe_2O_3 nano-phase in borate glasses doped with Fe and Gd, J. Magn. Magn. Mater 401 (2016) 880-889.

[18]   J.i. Tuček, R. Zbořil, A. Namai, S.-i. Ohkoshi, ε-Fe_2O_3: an advanced nanomaterial exhibiting giant coercive field, millimeter-wave ferromagnetic resonance, and magnetoelectric coupling, Chem. Mater. 22 (2010) 6483-6505.

[19]   S.N. Bahadur, A. Sonal, Nanocomposites: an overview, Emerging Mater. Res. 5 (2016) 5-43.

[20]   M. Mikhaylova, D.K. Kim, N. Bobrysheva, M. Osmolowsky, V. Semenov, T. Tsakalakos, M. Muhammed, Superparamagnetism of magnetite nanoparticles: dependence on surface modification, Langmuir 20 (2004) 2472-2477.

[21] J.L. Lyon, D.A. Fleming, M.B. Stone, P. Schiffer, M.E. Williams, Synthesis of Fe oxide core/Au shell nanoparticles by iterative hydroxylamine seeding, Nano Lett. 4 (2004) 719-723.

[22] D. Korte, G. Carraro, C. Maccato, M. Franko, Determination of thermooptical and transport parameters of ε iron(III) oxide-based nanocomposites by beam deflection spectroscopy, Opt. Mater. 42 (2015) 370-375.

[23] Z. Xu, Y. Hou, S. Sun, Magnetic core/shell Fe_3O_4/Au and Fe_3O_4/Au/Ag nanoparticles with tunable plasmonic properties, J. Am. Chem. Soc. 129 (2007) 8698-8699.

[24] Lingyan, Lingyan, J. Luo, Q. Fan, M. Suzuki, I.S. Suzuki, M.H. Engelhard, Y. Lin, N. Kim, J.Q. Wang, C.-J. Zhong, Monodispersed core−shell Fe_3O_4@Au nanoparticles, J. Phys. Chem. B 109 (2005) 21593-21601.

[25] C. Venkateswaran, D. Paul Joseph, R. Selva Vennila, Critical analysis on the structural and magnetic properties of bulk and nanocrystalline Cu-Fe-O, Adv. Mater. Sci. Eng. 2010 (2010)

[26] S.J. Stewart, R.A. Borzi, G. Punte, R.C. Mercader, F. Garcia, Microstructural and magnetic characterization of nanostructured α-Fe_2O_3 and CuO mixtures obtained by ball milling, J. Phys. Cond. Matter 13 (2001) 1743-1757.

[27] D. Barreca, P. Fornasiero, A. Gasparotto, V. Gombac, C. Maccato, T. Montini, E. Tondello, The potential of supported Cu_2O and CuO nanosystems in photocatalytic H_2 production, ChemSusChem 2 (2009) 230-233.

[28] D. Barreca, G. Carraro, E. Comini, A. Gasparotto, C. Maccato, C. Sada, G. Sberveglieri, E. Tondello, Novel synthesis and gas sensing performances of CuO–TiO_2 nanocomposites functionalized with Au nanoparticles, J. Phys. Chem. C 115 (2011) 10510-10517.

[29] Y.S. Chaudhary, A. Agrawal, R. Shrivastav, V.R. Satsangi, S. Dass, A study on the photoelectrochemical properties of copper oxide thin films, Int. J. Hydrogen Energy 29 (2004) 131-134.

[30] D. Barreca, A. Gasparotto, C. Maccato, E. Tondello, O.I. Lebedev, G. Van Tendeloo, CVD of copper oxides from a β-diketonate diamine precursor: tailoring the nano-organization, Cryst. Growth Des. 9 (2009) 2470-2480.

[31] D. Saberi, M. Sheykhan, K. Niknam, A. Heydari, Preparation of carbon nanotube-supported α-Fe_2O_3@CuO nanocomposite: A highly efficient and magnetically separable catalyst in cross-coupling of aryl halides with phenols, Catal. Sci. Technol. 3 (2013) 2025-2031.

[32] D. Barreca, G. Carraro, D. Peeters, A. Gasparotto, C. Maccato, W.M.M. Kessels, V. Longo, F. Rossi, E. Bontempi, C. Sada, A. Devi, Surface decoration of ϵ-Fe_2O_3 nanorods by CuO via a two-step CVD/sputtering approach, Chem. Vap. Deposition 20 (2014) 313-319.

[33] S. Sakurai, A. Namai, K. Hashimoto, S.-i. Ohkoshi, First observation of phase transformation of all four Fe_2O_3 phases ($\gamma \rightarrow \epsilon \rightarrow \beta \rightarrow \alpha$-phase), J. Am. Chem. Soc. 131 (2009) 18299-18303.

[34] H.S. Nalwa, Encyclopedia of Nanoscience and Nanotechnology, Volumes 1-10, American Scientific Publishers, Los Angeles CA, 2004.

[35] G. Carraro, A. Gasparotto, C. Maccato, E. Bontempi, O.I. Lebedev, C. Sada, S. Turner, G. Van Tendeloo, D. Barreca, Rational synthesis of F-doped iron oxides on $Al_2O_3(0001)$ single crystals, RSC Adv. 4 (2014) 52140-52146.

[36] G. Carraro, C. Maccato, E. Bontempi, A. Gasparotto, O.I. Lebedev, S. Turner, L.E. Depero, G. Van Tendeloo, D. Barreca, Insights on growth and nanoscopic investigation of uncommon Iron oxide polymorphs, Eur. J. Inorg. Chem. 2013 (2013) 5454-5461.

[37] D. Peeters, D. Barreca, G. Carraro, E. Comini, A. Gasparotto, C. Maccato, C. Sada, G. Sberveglieri, Au/ϵ-Fe_2O_3 Nanocomposites as Selective NO_2 Gas Sensors, J. Phys. Chem. C 118 (2014) 11813-11819.

[38] D. Barreca, G. Carraro, A. Devi, E. Fois, A. Gasparotto, R. Seraglia, C. Maccato, C. Sada, G. Tabacchi, E. Tondello, A. Venzo, M. Winter, β-Fe_2O_3 nanomaterials from an iron(II) diketonate-diamine complex: a study from molecular precursor to growth process, Dalton Trans. 41 (2012) 149.

[39] D. Barreca, A. Gasparotto, E. Tondello, C. Sada, S. Polizzi, A. Benedetti, Nucleation and growth of nanophasic CeO_2 thin films by plasma-enhanced CVD, Chem. Vap. Deposition 9 (2003) 199-206.

[40] D. Briggs, M.P. Seah, Practical surface analysis: Auger and X-ray photoelectron spectroscopy, John Wiley & Sons: New York, 2nd ed., 1990.

[41] J.F. Moulder, W.F. Stickle, P.E. Sobol, K.D. Bomben, Handbook of X-ray photoelectron spectroscopy, Perkin Elmer Corperation, Eden Prairie, MN, USA, 1992.

[42] D.A. Shirley, High-resolution X-ray photoemission spectrum of the valence bands of gold, Phys. Rev. B 5 (1972) 4709.

[43] C.D. Wagner, A. Joshi, The auger parameter, its utility and advantages: a review, J. Electron. Spectrosc. Relat. Phenom. 47 (1988) 283-313.

[44]   G. Moretti, Auger parameter and Wagner plot in the characterization of chemical states by X-ray photoelectron spectroscopy: a review, J. Electron. Spectrosc. Relat. Phenom. 95 (1998) 95-144.

[45]   http://srdata.nist.gov/xps.

[46]   Pattern N° 51122, ICSD (**2007**).

[47]   R.A. Laudise, Treatise on Solid State Chemistry, Plenum Press, New York, 1975.

[48]   Y. Pan, Y. Gao, G. Wang, D. Kong, L. Zhang, J. Hou, S. Hu, H. Pan, J. Zhu, Growth, structure, and stability of Au on ordered $ZrO_2(111)$ thin films, J. Phys. Chem. C 115 (2011) 10744-10751.

[49]   S.-i. Ohkoshi, H. Tokoro, Hard Magnetic Ferrite: ε-Fe_2O_3, Bull. Chem. Soc. Jap. 86 (2013) 897-907.

[50]   K.-h. Zhong, Z.-g. Huang, Z.-g. Chen, Q. Feng, Y.-m. Yang, Numerical calculation of magnetization behavior for Co nanowire array, Trans. Nonferrous Mat. Soc. China 18 (2008) 700-706.

[51]   E.P. Wohlfarth, Relations between different modes of acquisition of the remanent magnetization of ferromagnetic particles, J. Appl. Phys. 29 (1958) 595-596.

[52]   P.E. Kelly, K.O. Grady, P.I. Mayo, R.W. Chantrell, Switching mechanisms in cobalt-phosphorus thin films, IEEE Trans. Magnet. 25 (1989) 3881-3883.

[53]   D. Peddis, P.E. Jonsson, G. Varvaro, S. Laureti, In Nanomagnetism: Fundamentals and Applications, Binns, C., Ed. Elsevier B.V: Oxford, UK, 2014; pp 129–189.

[54]   G. Muscas, P. Anil Kumar, G. Barucca, G. Concas, G. Varvaro, R. Mathieu, D. Peddis, Designing new ferrite/manganite nanocomposites, Nanoscale 8 (2016) 2081-2089.

[55]   J. Jin, S. Ohkoshi, K. Hashimoto, Giant coercive field of nanometer-sized iron oxide, Adv. Mater. 16 (2004) 48-51.

Captions for Figures

Figure 1. XRD patterns for ε-Fe$_2$O$_3$ specimens deposited on Si(100) substrates. The pattern related to bare iron(III) oxide is also displayed for comparison.

Figure 2. Representative plane-view and cross-sectional FE-SEM images for ε-Fe$_2$O$_3$-based nanocomposites.

Figure 3. Surface wide-scan XP spectra for ε-Fe$_2$O$_3$ composite specimens. The corresponding (a) Fe2p, (b) Au4f and (c) Cu2p photoelectron signals are displayed as insets.

Figure 4. Room temperature field-dependent magnetization loops for samples: (a) ε-Fe$_2$O$_3$-Au, and (b) ε-Fe$_2$O$_3$-CuO, recorded with the external magnetic field applied either parallel (open circles) or perpendicular (closed circles) to the rod axis.

Figure 5. Schematic view of ε-Fe$_2$O$_3$ crystallographic structure oriented along the [013] direction with respect to the substrate surface. The magneto-crystalline easy-axis ($\equiv a$ axis) lies in the substrate plane (*i.e.*, along the normal to the rod axis).

Figure 6. (a) Comparison between the IRM (closed circles) and DCD (open circles) remanence curves for the ε-Fe$_2$O$_3$-Au sample; the curves are normalized to the remanent moment measured after applying an external field of 2T (m_r/m_r^{2T}). (b) δM plot derived from the remanence curves.

Figure 7. (a) Set of DCD curves of sample Fe$_2$O$_3$-Au measured with the external field applied at different ϕ angles with respect to the substrate surface. (b) Angular dependence of the experimental normalized remanence coercivity $H_{cr}(\phi)/H_{cr}(0°)$.
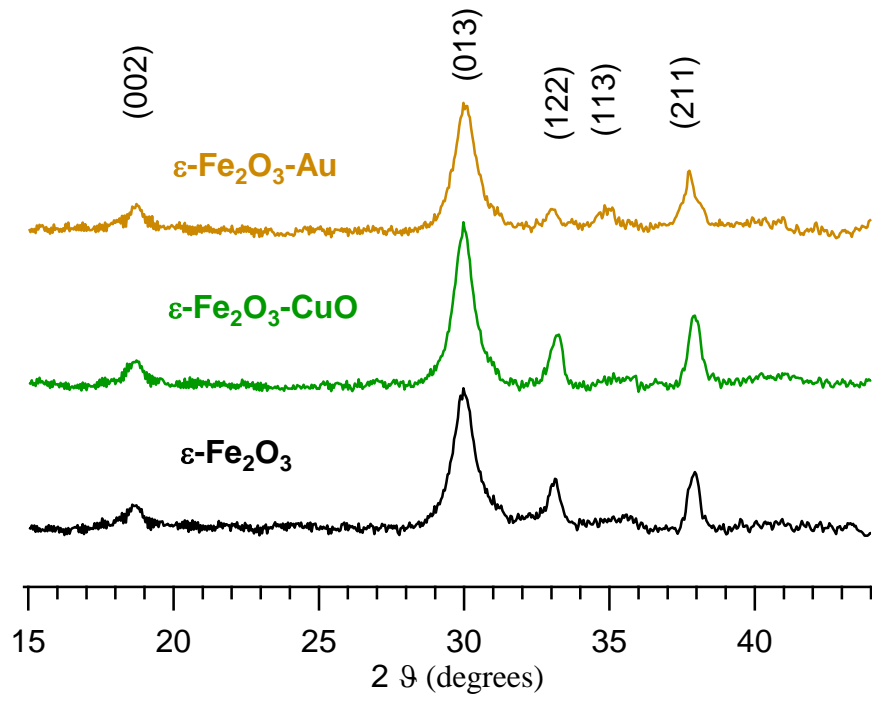
Figure 1

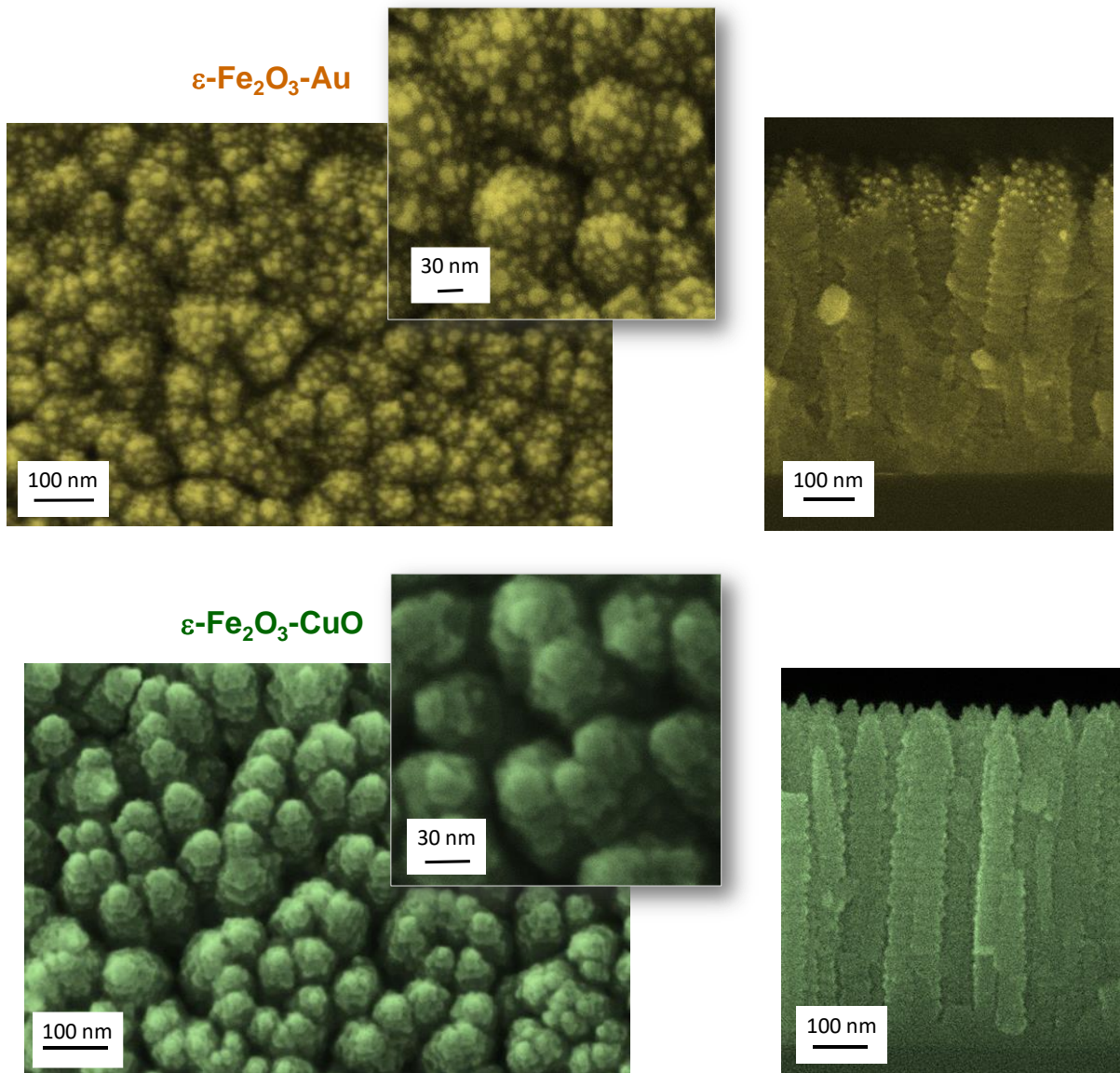by G. Carraro *et al.*

Figure 2

by G. Carraro *et al*.

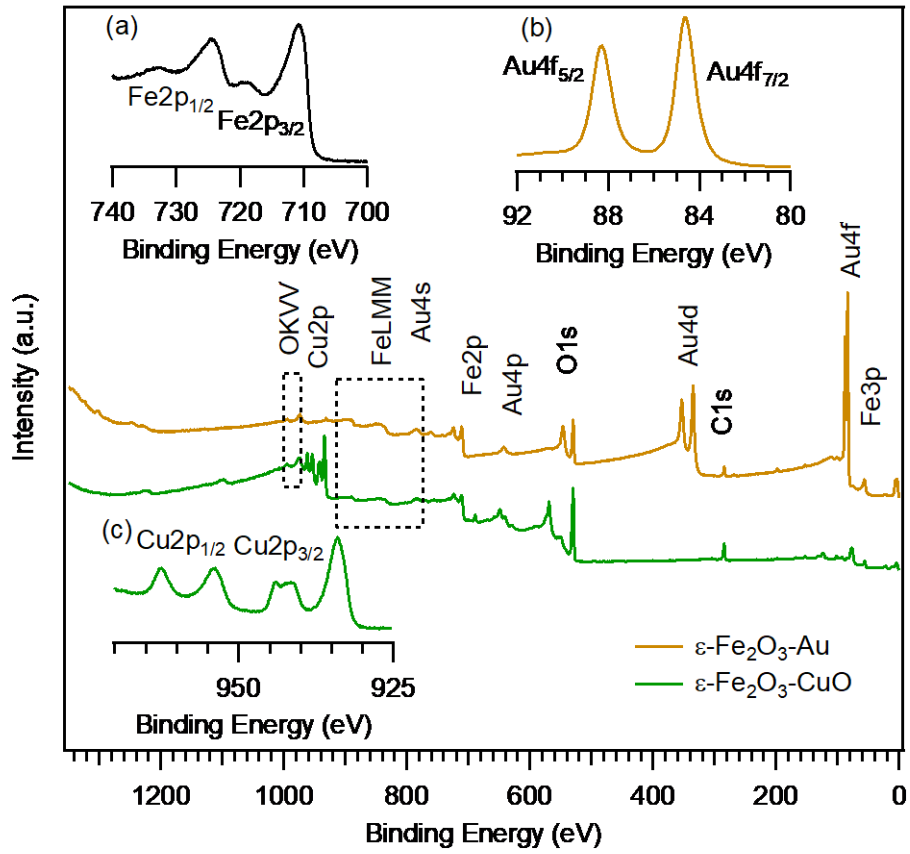ε-Fe₂O₃-Au

ε-Fe₂O₃-CuO

Figure 3

by G. Carraro *et al.*

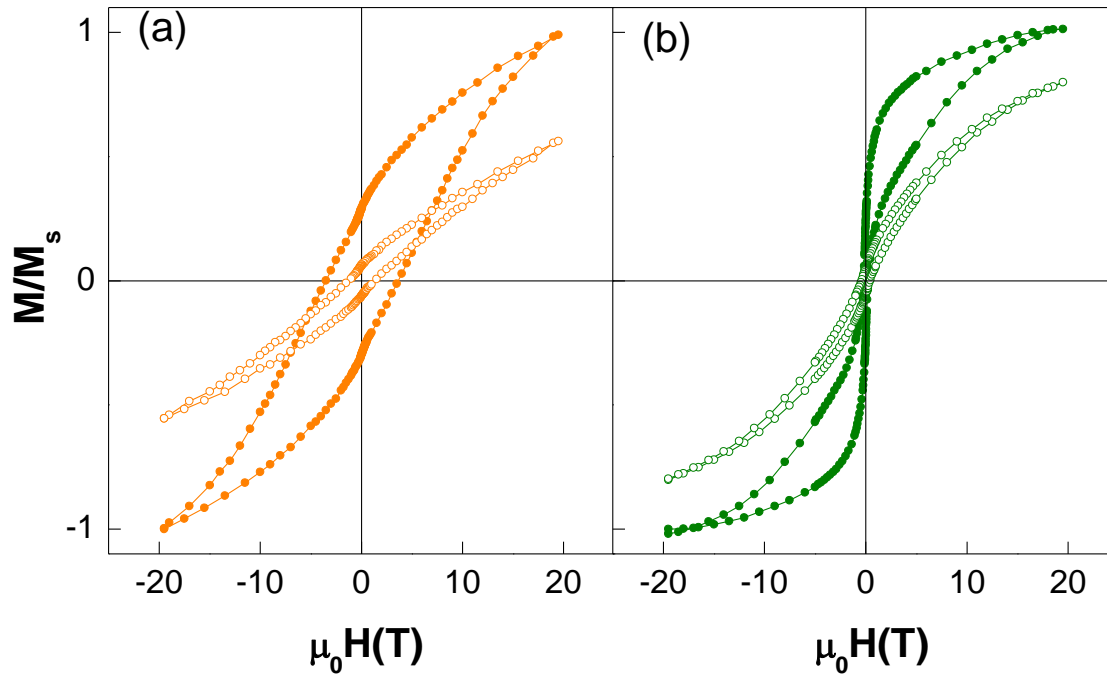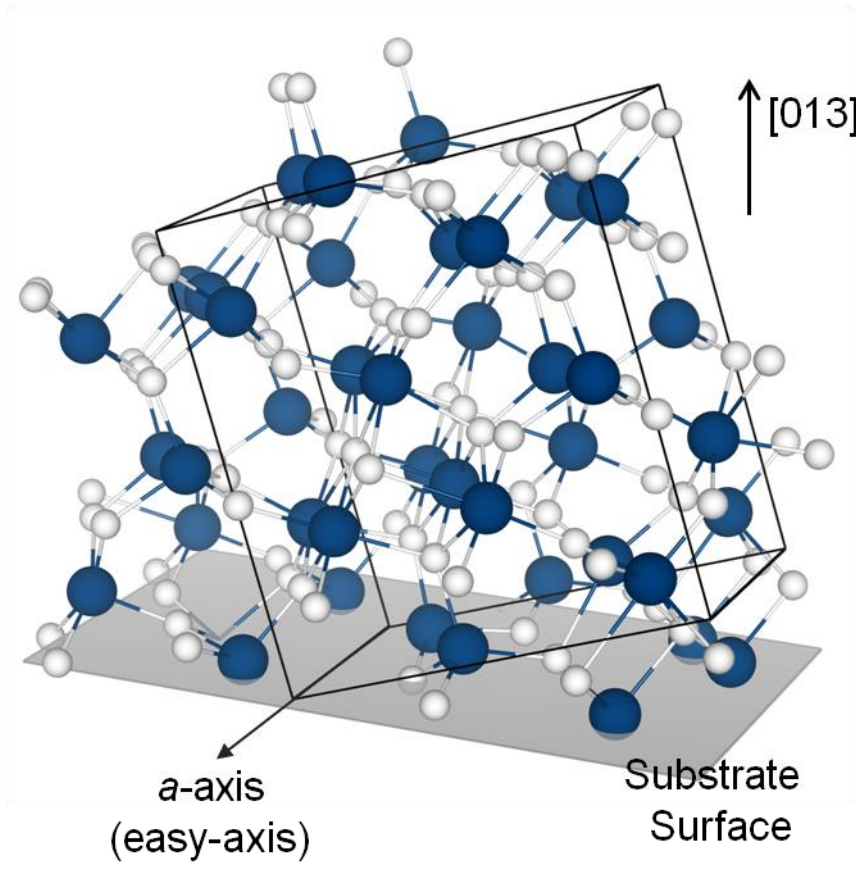**Figure 4**

by G. Carraro *et al.*
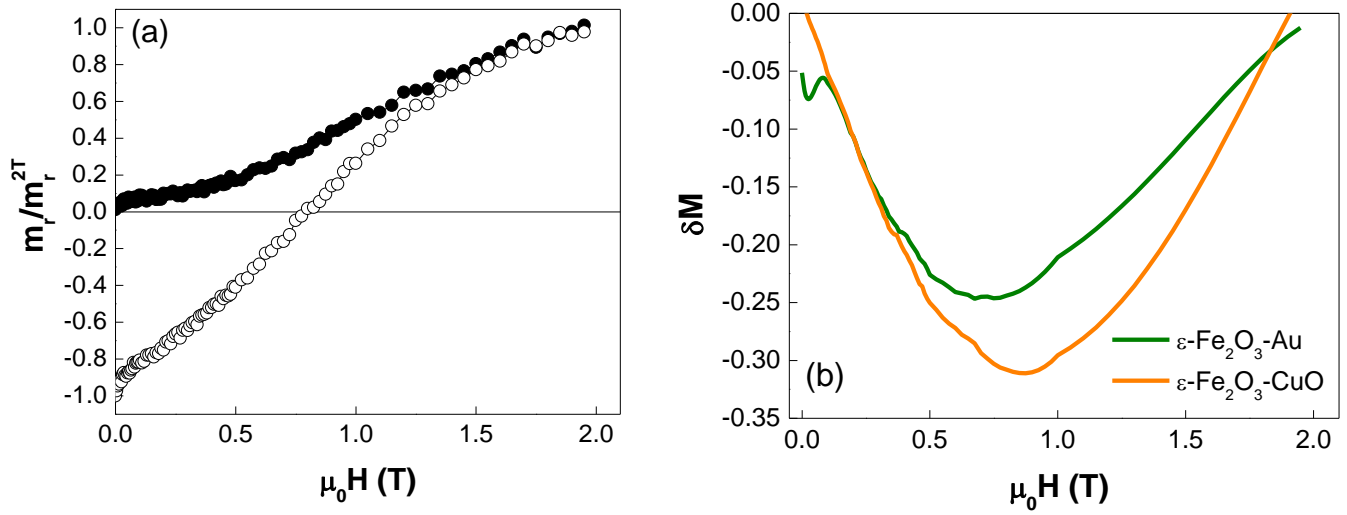
Figure 5

by G. Carraro *et al.*

Figure 6

by G. Carraro *et al.*

Figure 7

by G. Carraro *et al.*